TELKOMNIKA Indonesian Journal of Electrical Engineering
Vol.10, No.5, September 2012, pp. 1005~1014

Segmentation Lung Fields in Thoracic CT Scans using Manifold Method

Jun Lai[1,2], Mei Xie[1]
[1]School of Electronic Engineering, University of Electronic Science and Technology of China
ChengDu, 610054, China
[2]School of Computer Science and Technology,ChongQing University of Posts and
Telecommunication,ChongQing, 400065, China
e-mail: laijun@cqupt.edu.cn

Abstract

*When the pathologies are in the close vicinity of the lung wall, the acquisition of the pulmonary nodules depends on accurate segmentation of the lung fields. However, the traditional methods based on pixels intensity cannot segment out them correctly. The paper proposes an effective segmentation method based on primary component analysis (PCA) manifold. It used the lung fields' relationship in a lung to construct the shape manifold with **B**-spline interpolation. In the manifold space, according to the position of the affected lung field, a measurement had been used to find an amended position, and it was projected back into the shape space to reconstruct the prior shape. The shape was registered with the affected one and then segmented the original lung section to obtain the correct lung field. The experiment results illustrate that the proposed method has more correct segmentation ability than the methods based on rolling-ball and pixel intensity.*

Keywords*: lung fields; high density pathologies; PCA manifold; segmentation.*

1. Introduction

The mortality rate for lung cancer is higher than other kinds of cancers around the world [1], [2], while detection in the early stages of cancer can be considered the most effective way to improve survival [2]. Computed tomography (CT) is the most sensitive imaging technique for detecting lung nodules and CT can provide high spatial and high temporal resolution, excellent contrast resolution for the pulmonary structures [3],[4]. In the medical image processing, segmenting the target object is a very important, and It is the prerequisitesto analyze the objects [5-7]. However, lung nodule detection is a challenging task in medical imaging as lung nodules are difficult to detect due to low contrast, small size, or the location of the nodule [8-12]. Moreover, accurate segmentation of lung tissues from low dose CT images is a more challenging problem and the segmentation of the region of interest (ROI) based on CT value has some problems for extracting abnormal area of the chest [13]. With the increased number of sections per scan, it is crucial to develop accurate and automated algorithms to deal with the difficult task of lung border delineation [14-17]. The computer assistant diagnosis for the pulmonary nodules also requires accurate segmentation of lung field. However, many segmentation methods rely on a large contrast between the lung field and surrounding tissues [8-13]. Most of the approaches would fail when the lung fields are affected by the high density pathology close to the lung wall [18-20]. Armato et al had used the rolling ball algorithm to overcome the loss of juxta-pleural nodules in the segmentation [19], But the problem has not been solved properly. Especially when the high density nodules are big in size, it is difficult problem to choose the radius of the rolling ball. Wang et al try to identify surrounding structures with extra information, such as the rib cage and the diaphragm [20]. Unfortunately, at most situations, it is unsuccessful because the chest CT is too complex to implement. This paper proposes a novel segmentation method based on the shape manifold [21–23], and the method can outperform the mentioned methods for it enforces the available prior knowledge of the lung volume.

This paper is organized as follows. In section 2, the PCA manifold construction method is given, and the lung field shape reconstruction based on the manifold is presented. The

Received June7, 2012; Revised September2, 2012; Accepted September 11, 2012

experimental results of comparing the proposed algorithm with other algorithms are presented in section 3. Finally, the conclusion summarize the paper in the last section.

2. Research Method

2.1. Construction PCA Manifold

The exterior smooth surface of a lung in a three-dimension space can be used as the prior knowledge for the lung fields segmentation. According to a lung anatomic structure, in a lung, the lung surface is smooth and the lung fields boundaries are constrained by the axis surface. In other word, their profiles are limited by the intersecting lines of the surface of the lung volume and the planes of the lung field. When the profiles in a lung are considered as the whole, they form the similarity manifold. A lung field can be seen as a two-dimensional m×m array, and it may also be considered as a vector of dimension m^2×1.So *n* lung fields in a lung can be denoted by the vectors set $Z = \{z_1, z_2, ..., z_n\} \subset R^{m^2 \times n}$, and the covariance matrix of the vectors is defined as follows:

$$M = \frac{1}{n}\sum_{i=1}^{n}(z_i - \hat{z})(z_i - \hat{z})^T \quad (1)$$

Where $\hat{z} = (z_1 + z_2 + ... + z_n)/n$, T denotes the transpose of a vector. The eigenvalues and eigenvectors of the covariance M are calculated, and let the set $U = \{u_1, u_2, ..., u_r\} \subset R^{m^2 \times r}$ $r<n$ includes the r eigenvectors corresponding to the r largest eigenvalues. Let U^T is the transpose matrix of the eigenvectors U, and the vector of the lung field in original space can be expressed as $Z \subset R^{m^2 \times 1}$. Thus, their corresponding eigenvector-based d-dimensions coordinates $V \subset R^{d \times r}$ can be obtained by:

$$V = U^t Z \quad (2)$$

For example, twenty lung fields in a lung are shown in the Fig. 1, and their position coordinates of the lung fields in low dimension space can be obtained by the PCA dimensionality reduction. The PCA coordinates of the lung fields have been show in the Fig. 2. In the diagram, every circle denotes the two or three-dimensional coordinate expression of a lung field and the number beside it is the corresponding sequential label.

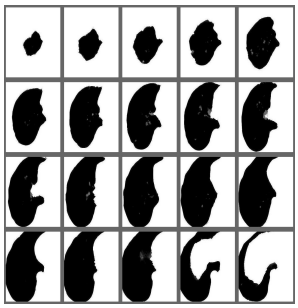

Figure 1. Lung fields in a lung

The position coordinates, which are acquired from the lung fields, scatter along the smooth manifold and the sequential numbers associated with the variation trend of the manifold. The lung fields are high dimensional, but their intrinsic dimensionality is low. When their relationship has been transformed into a lower-dimensional space, especially a visual manifold

space of two dimensions and three dimensions, it is easier for ones to find the underlying relationship of the lung fields.

Supposing that a smooth curve can denote the manifold, it can be constructed by the *B*-spline interpolation. The lung fields positions are expected in equal interval, but the small deviation does not influence the manifold construction. Let the spline-order *d* equals 4, in order to make the construction curve keep the curvature smooth character, and the manifold curve can be written as:

$$t:[0,1]\to\Omega, \qquad P(t)=\sum_{n=0}^{N-1} p_n B_{n,\ 4}(t) \tag{3}$$

where *N* is the total number of the lung fields, $B_{n,d}$ (*n* = 0,1,2,…, *N*-1, *d* = 4) is a mixture function, and it is periodic *B*-spline basis functions [24]. The curve of the manifold can be denoted as *P*(*t*), all points on the curve would be well suited for the representing of lung fields.

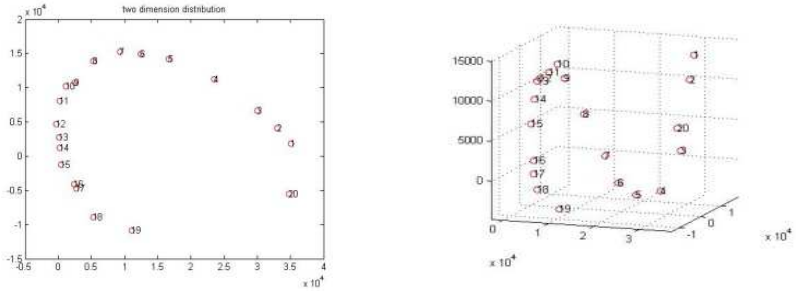

(a) (b)

Figure 2. points distribution in the low dimension space

However, when some lung fields in a lung have been affected by a nodule ball close to the thoracic wall, the affected lung fields positions have been chosen as basic construction points, and the construction manifold would not keep smoothly characters. Therefore, for to solve this problem, two rules are introduced: (1) the area variation character of the lung fields. In a lung, the area differences between two adjacent lung fields would show a special variation trend, and the character is used for the construction points choosing. The area differences of two adjacent lung fields can be computed by:

$$dA_{LF[i,j]}=A_{LF[i]}-A_{LF[j]} \qquad i<j \tag{4}$$

where $dA_{LF\,[i,j]}$, $A_{LF\,[i]}$ and $A_{LF\,[j]}$ denotes the difference area between the *i*-th, *j*-th lung fields, the area of *i*-th and *j*-th lung field respectively. Assuming that *k* is the label of the maximum area lung field in the lung, from apex to the *k*-th lung field, the area difference is position; and from the *k*-th lung field to lung bases, it is negative. And they content with the relationship:

$$\begin{aligned} A_{LF[i]} &\le A_{LF[j]} \qquad i<j<k \\ A_{LF[i]} &\ge A_{LF[j]} \qquad k<i<j \end{aligned} \tag{5}$$

(2) the slow curvature variation character. The curvature on the smooth manifold is slowly varying, and when the t has a defined value t0 the curvature of a point can be computed by:

$$\kappa=\left|\mathrm{P}'(t)\times\mathrm{P}''(t)\right|/\left|\mathrm{P}'(t)\right|^3 \tag{6}$$

where *P*(*t*) is defined in (3), The apostrophes are one or two order derivation operator respectively. One of many lung fields affected by a nodule sphere is shown in figure 3(a), and based on the above construction points choosing rules, the manifold has been constructed as shown in Fig.3(b). Motivated by the principle of PCA manifold, the neighborhood relationships, which are kept un-changed during dimensionality reduction, should be used to acquire the approximate shape for the affected lung field.

2.2. Affected Shape Reconstruction

When a lung field is affected by a high density pathology close to the lung wall, the corresponding shape PCA position must deviate away from the normal manifold. It can not denote the real lung field coordinates, therefore, the deviated position should be amended with the closest position on the manifold.

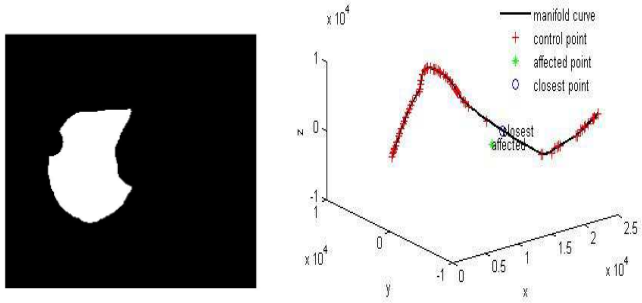

Figure 3. An affected lung field and the position

Then, the amended position would be projected back into the original shape space to acquire the prior shape. And the 2-norm measurement has been introduced to judge the deviation distance as:

$$\text{dist} = \left\| \text{p}_{\text{manifold}} - \text{p}_{\text{deviate}} \right\|^2 \tag{7}$$

When *dist* is greater than the pre-set threshold, the closest position would be obtained. Supposing an affected position can be expressed as (8), the parameter *u* of the closest point can be computed by the (9).

$$Q_0 = \left(x_0, y_{0,} z_0 \right)^t \tag{8}$$

$$u_0 = \arg\min_u \{ \| Q_0 - C(u) \| \} \tag{9}$$

Where *P*(*u*) is similarity as (3). When the variable *u* has a defined value u_0, the closest position $P(u_0)$ can be computed. And the closest position also can be acquired by the geometric method. Let us introduce the equation (11), and the $N(u_0)$ is the unit tangent vector on the assuming closest point $P(u_0)$ which can be computer by (10). And the line segment between the Q_0 and $P(u_0)$, must lies on the flat plane expressed as (11). Combined with the (3), the parameter value u_0 and $P(u_0)$ can be determine.

$$N\left(u_0\right) = C^{'}(u_0) / \left| C^{'}(u_0) \right| \tag{10}$$

$$N(u_0)(p(u_0) - Q_0) = 0 \tag{11}$$

From the position $P(u_0)$, let U^T denote the transpose inverse of the U matrix, and the prior shape L of the affected lung field can be obtained by:

$$L = U^T p(u_0) \tag{12}$$

Following above method, the manifold has been reconstructed and one prior shape of the lung fields affected by the high density nodule close to the lung wall has been obtained. The original shape, reconstruction shape, the difference of the original, reconstruction shape and the affected shape have been shown in the Fig. 4 respectively.

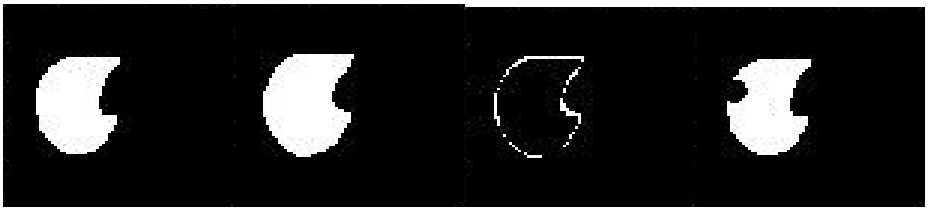

(a) (b) (c) (d)

Figure 4. (a) original; (b) reconstruction;(c) difference; (d) affected.

3. Results and Analysis

Low dose lung CT series have been acquired from PCsub1-20090909 dataset provided by Cornell university, and each series set has about two hundreds lung field images, which had been scanned in 1.25mm interval. In the experiment, the simulation data is obtained in the following ways: firstly, for reducing the computational complexity, these CT series have been down-sampled to half of the original series in size, and excluded the images that don't meet the two conditions as described in section 2. Secondly, for testing the proposed method, the ball-shape nodules have been placed into the lung fields. The center of the nodules ball is placed on or close to the convex edges of the lung fields and the setting parameters of the placed nodules as shown in table 1.

Table 1. The datasets and placed parameters

Cases	Lung CT series	Center Coordinates of the Nodule Sphere	Nodule Radius(pixels)
W0001	256*256*170	130,46,60	5-25
W0002	256*256*160	133,47,60	5-25
W0003	256*256*151	109,45,60	5-25
W0004	256*256*151	125,32,60	5-25
W0005	256*256*168	113,43,60	5-25
W0006	256*256*168	137,212,60	5-25
W0007	256*256*148	140,208,60	5-25
W0009	256*256*149	132,211,60	5-25
W0010	H256*256*149	113,214,60	5-25

3.1. Manifold Construction

The left lung fields and right lung fields in the W0001, W0002 are placed with the nodule ball, whose radius is 15 pixels and center is set as Table 1 respectively. Following the described method in section 2, four pulmonary manifolds have been constructed as figure 5-6. The green smooth curve and red 'o' points denote the reconstruction manifold and control points respectively. Each lung fields series form the different manifolds, but the manifolds have some similarity on the shape, and they have verified that the manifold reconstruction method is feasible.

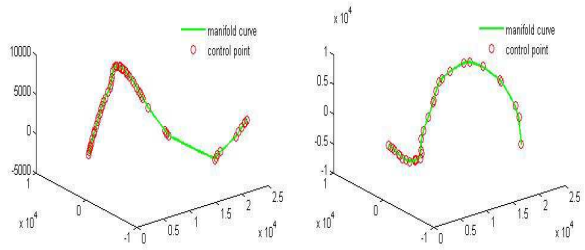

Figure 5. (a) W0001 left; (b) W0001 right

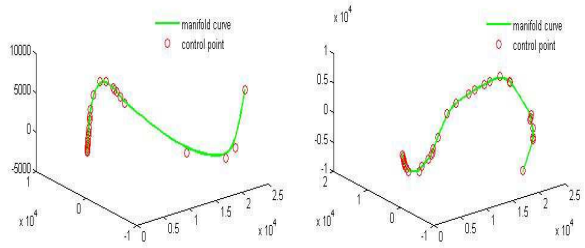

Figure 6. (a) W0002 left; (b) W0002 right

3.2. Prior Shape Reconstruction, Registration and Segmentation

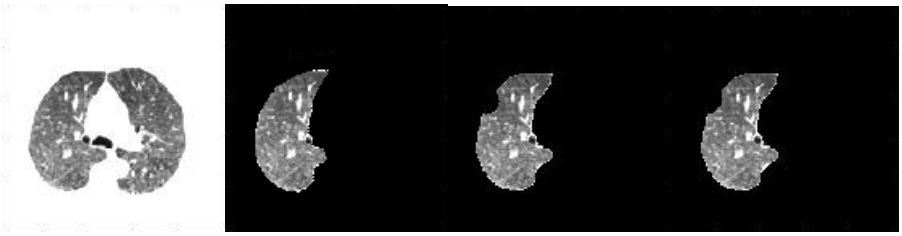

(a) (b) (c) (d)

Figure 7. the 80th left lung field in W0002

When the distant between the position of the affected shape and the manifold is greater than the pre-set threshold (default is 0.1), the amended position would be obtained by described method in section 2. For example, in Fig. (a), the left lung field in W0002 has been placed with the nodule ball, whose radius is 15 pixels and center is on the 80th lung field. In the proposed method, the prior approximate shape has been reconstructed, and then it registers with the affected shape by the minimum distant match for harris features [25]. And it is used to segment out the lung field from the lung section as shown in Fig. 7(b). Let the radius of the rolling ball equals that the nodule radius multiplies a constant factor(the factor is 1.2), and the segmentation result toward the same section by the methods based on pixels intensity and rolling ball has been shown in Fig. 7(c) and Fig. 7(d) respectively.

Observing the result, ones can see that, even if a lung field edge badly influenced by the pathology, the prior shape can be well acquired by the proposed method.

3.3. Statistics Comparison

In order to evaluate the proposed method, let '| |' denote the absolute value operation, a relative error about the region area is introduced as:

$$e = \left| A_o - A_r \right| / A_o \times 100\% \quad (13)$$

where the e, A_o, A_r is the relative error rate, the original area and the segmentation area of the lung field respectively.

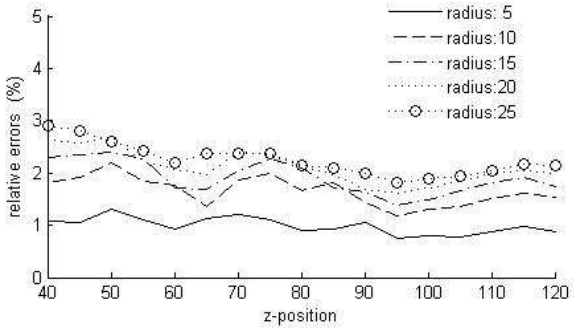

Figure 8. W0001 left lung field segmentation

Table 2.left lung field in W0001-W0005

Dataset	Radius (pixels)	Real Area	Method		
			Intensity	Ball	Manifold
W0001	5	7175	7152	7417	7202
	10		7024	7351	7221
	15		6825	7081	7275
	20		6561	6981	7371
	25		6235	6700	7430
W002	5	6583	6542	7046	6722
	10		6419	7011	6625
	15		6220	6723	6709
	20		5949	7069	6857
	25		5608	6819	6820
W0003	5	6317	6273	6716	6581
	10		6155	6655	6497
	15		5966	7523	6327
	20		5707	7683	6550
	25		5381	8149	6574
W0004	5	10870	10818	11061	11126
	10		10685	10974	11163
	15		10474	10934	11156
	20		10195	12044	10991
	25		9849	12203	11115
W0005	5	7286	7275	7598	7345
	10		7165	7556	7531
	15		6983	7315	7297
	20		6735	7059	7382
	25		6424	6732	7302

The left lung fields in W0001 CT series have been placed with the different nodule-balls respectively, And the center position of the ball changes from 50 to 100 along *z*-direction while the radius changes from 5 to 25 pixels. The testing results have been shown in Fig. 8. From the diagram, with nodule radius increasing, the segmentation error is increasing gradually. However, with the center position of nodule ball varying along the *z*-axis position direction, the segmentation error decrease a little gently.

To further verify the proposed method in quantity, the more testing lung fields are listed in table1. When the radius of the rolling-ball is fixed as 15 pixels, the experiment results have been shown in Table 2 and Table 3.

For understanding the overall effect of the proposed method in Table2 and Table3, these data have been summed and averaged depending on the different radius of the nodules respectively, and their relative errors have been shown in Fig. 9.

Table 3. Some right lung field in W0006-W0010

Dataset	Radius (pixels)	Real Area	Methods		
			Intensity	Ball	Manifold
W0006	5	6080	6046	652	6110
	10		5928	9	6330
	15		5739	647	6291
	20		5491	6	6176
	25		5184	652	6369
				0	
				665	
				7	
				643	
				1	
W007	5	7025	7006	7469	7036
	10		6885	7383	7165
	15		6692	7137	7147
	20		6433	6872	7269
	25		6110	6526	7279
W0009	5	7905	7869	750	7975
	10		7742	3	8089
	15		7546	741	8073
	20		7282	9	8148
	25		6948	724	8172
				3	
				699	
				8	
				669	
				8	
W0010	5	6915	6887	734	7142
	10		6776	7	6998
	15		6601	726	7119
	20		6373	6	7112
	25		6088	706	6964
				8	
				683	
				6	
				653	
				9	

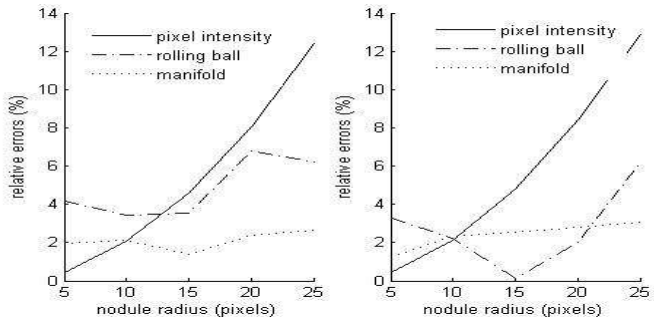

Figure 9. Relative errors (a) W0001-5; (b)W0006-10

Comparing the results in Fig. 9, the error based on pixels intensity is quickly increasing with increaseing of the nodule radius, and the error based on rolling ball is varying with changing of the rolling-ball. In the diagram, the proposed method error is less than the rolling ball and the pixel intensity threshold, and it is increasing slowly with the nodule radius increasing. The phenomenon steming from the manifold method has used the prior knowledge about the lung volume, so that it can get more reasonable results and has a small relative error than the others.

4. Conclusion

This paper presents a segmentation method for lung fields based on the shape manifold, and it consists of PCA dimension reducing, manifold reconstructing, position amending, prior shape acquiring and segmenting steps. The experiment results show that the proposed method can obtain some good segmentation results and it is also capable of improving the segmentation accuracy for the lung fields affected by the high density pathologies close to the thoracic wall. For it has considered the position, shape of the lung field in a lung to acquire a better prior shape for the affected one, the segmentation results are more accurate and appropriate than the other methods. Although the errors is still larger in the region area, it can improve the segmentation results especially for the juxta-pleural nodules. However, the proposed method still has an unsolved problem: when the lung fields in the apex or base of the lungs has been affected by the thoracic high density pathologies, the prior shape can not be acquired by the proposed method in general.

Acknowledgments

Authors are grateful for University of Cornell to provide lung CT PCsub1-20090909 dataset. And this work was supported in part by NSFC under Grant Nos. 61171060and foundation of Chongqing University of Posts and Telecommunications, China (A2009-58).

References

[1] McCulloch CC, Kaucic RA, Mendonca PRS. Model-based Detection of Lung Nodules in Computed Tomography Exams1- Thoracic Computer-aided Diagnosis. *Acad Radiol.* 2004; 11(3): 258-266.
[2] Dehmeshiki J, Amin H, Valdivieso M. Segmentation of Pulmonary Nodules in Thoracic CT Scans: A Region Growing Approach. *IEEE T MedImaging*. 2008; 27(4): 4-27.
[3] Diciotti S, Picozzi G, Falchini M. 3-D Acquiring Algorithm of Small Lung Nodules in Spiral CT Images. *IEEE T Inf. Technol B.* 2008; 12(1): 7-19.
[4] Hu S, Hoffman EA, Reinhardt JM. Automatic Lung Segmentation for Accurate Quantization of Volumetric X-Ray CT Images. *IEEE T Med Imaging*. 2001; 20(6): 490-498.
[5] H. Tjandrasa, A. Wijayanti, N. Suciati. Segmentation of the Retinal Optic Nerve Head using Hough Transform and Active Contour Models. *TELKOMNIKA Indonesian Journal of Electrical Engineering*. 2012; 10(3): 489-596.
[6] J. Sun, Y.Wang, X. Wu etc. A New Image Segmentation Algorithm and It's Application in Lettuce Object Segmentation. *TELKOMNIKA Indonesian Journal of Electrical Engineering*. 2012; 10(3): 497-504.
[7] A. Alfiansyah, A Unified Energy Approach for B-Spline Snake in Medical Image Segmentation. *TELKOMNIKA Indonesian Journal of Electrical Engineering*. 2010; 8(2): 175-186.
[8] Soleymanpour E, Pourreza HR, Ansaripour E, Fully Automatic Lung Segmentation and Rib Suppression Methods to Improve Nodule Detection in Chest Radiographs, *Journal of Medical Signals and Sensors*. 201; 1(3).
[9] Retico A, Delogu P, Fantacci ME, Lung Nodule Detection in Low-dose and Thin-slice Computed Tomography. *Comput Biol Med.* 2008; 38(4): 525-534.
[10] Yim Y, Hong H. Correction of Segmented Lung Boundary for Inclusion of Pleural Nodules and Pulmonary Vessels in Chest CT Images. *Comput Biol Med.* 2008; 38(8): 845-857.
[11] Riccardi A, Petkov TS, Ferri G. Computer-aided detection of Lung Nodules via 3D Fast Radial Transform, Scale Space Representation, and Zernike MIP Classification. *Med Phys*. 2011; 38(4): 1962-1971.
[12] Way TW, Sahiner B, Chan HP. Computer-aided Diagnosis of Pulmonary Nodules on CT Scans: Improvement of Classification Performance with Nodule Surface Features. *Med Phys*. 2009; 36(7): 3086-3098.

[13] Itai Y, Kim H, Ishikawa S. A Segmentaion Method of Lung Areas by using Snakes and Auotmatic Detection of Abmormal Shadow on the Areas. *Int. J Innov Comput I*. 2007; 3(2): 277-284.
[14] Korfiatis P, Spyros S, Sakellaropoulos P. *Automated 3D Segmentation of Lung Fields in Thin Slice CT*,CAIP 2007, Berlin Heidelberg, 2007; LNCS 4673: 237-244.
[15] Way TW, Hadjiiski LM, Sahiner B. Computer-aided Diagnosis of Pulmonary Nodules on CT Scans: Segmentation and Classification using 3D Active Contours. *Med. Phys*. 2006; 33(7): 2323-2337.
[16] Ukil S, Reinhardt JM. Smoothing Lung Segmentation Surfaces in 3D X-ray CT Images using Anatomic Guidance. *Acad Radiol*. 2005; 12(10): 1502–1511.
[17] Sluimer I, Prokop M, Ginneken BV. Toward Automated Segmentation of the Pathological Lung in CT. *IEEE T Med Imaging*. 2005; 24(8): 1025-1038.
[18] Sluimer I, Schilham A, Prokop M. Computer Analysis of Computed Tomography Scans of the Lung: A Survey. *IEEE T Med Imaging*. 2006; 25(4): 385-405.
[19] Armato SG, Giger ML, Moran CJ. Computerized Detection of Pulmonary Nodules on CT Sans. *Radio Grphics*.1999; 19(5): 1003-1011.
[20] Wang O, O'Dell WG. Auto-segmentation of Juxta-Pleural Lung Fields in Chest CT Using Lung Contour Corrected by Anatomic Landmarks. Technical Report, University of Rochester Medical Center, Rochester, NY USA. 14642, 2004.
[21] Zhang C, Wang J, Zhao N. Reconstruction and Analysis of Multi-pose Face Images based on Nonlinear Dimensionality Reduction. *Pattern Recogn*. 2004; 37(7): 325-336.
[22] Roweis ST and Saul LK. Nonlinear Dimensionality Reduction by Locally Linear Embedding. *Science*. 2000; 290(22): 2323-2326.
[23] Tenenbaum JB, Silva VD, Langford JC. A Global Geometric Framework for Nonlinear Dimensionality Reduction. *Sicence*. 2000; 290(22): 2319-2323.
[24] Hearn D et al. Computer Graphics (Third Edition). Publishing House of Electronics Industry. Beijing, China. 2004.
[25] Schmid C, Mohrand R, Bauckhage C. Evaluation of Interest Point Detectors. *Int. Journal of Computer Vision*. 2000; 37(2): 151-172.